Research on Key Technologies of Terminals for Electric Power Satellite IoT Private Network System

(IJCSNT) International Journal of Communication Systems and Network Technologies
ISSN Number: 2053-6283
Volume 14, Issue No. 2, 97–107

https://journals.mirlabs.in/index.php/ijcsnt
DOI-10.18486/ijcsnt/14.2.009
IJCSNT

Gang Liang[1], Yongbo Yao[2], Peng Xie[3], Xin Wang[4], Jie Liu[5], Wei Zhang[6], Gang Zhao[7]

Abstract

To address the monitoring requirements of transmission lines in areas without public network coverage in Xinjiang, an integrated electric power satellite IoT terminal is developed. Using a GaN power amplifier and a three-level sleep/wake-up mechanism, the operating power consumption is $\leq$30W, standby is $<$1W, achieving 94.6% energy saving. Forward link uses QC-LDPC+BPSK, return link uses Turbo+QPSK+12x spreading, achieving a demodulation threshold as low as $-$17dB, meeting the $-$12dB target. Simulation verifies an end-to-end delay of 90-115ms, meeting the real-time requirements of electric power services.

Keywords

Satellite IoT, Low Power Consumption, Low Demodulation Threshold, Anti-Interference Coding, GEO Satellite

Received: 14 May 2025; **Revised:** 30 July 2025; **Accepted:** 04 August 2025;
Published: 31 August 2025;

[1, 2, 4, 5, 6, 7]State Grid Xinjiang Information & Telecommunication Company, State Grid Xinjiang Electric Power Co., Ltd, Urumqi, China.
[3]State Grid Xinjiang Electric Power Co., Ltd, Urumqi, China.

Corresponding author:
Email: tla02@126.com

Introduction

With the advancement of the "Dual Carbon" strategy, Xinjiang, as a core base for "West-to-East Power Transmission", needs to transmit large-scale power to Central China, East China, and other regions[1–3]. However, transmission lines often traverse extreme environments such as deserts, Gobi, high-cold regions, and sandstorms. Many monitoring and collection points are located in areas without public network coverage, making traditional communication deployment impossible. Manual inspection poses significant risks such as power grid loss of control and energy efficiency failure[4–6].

Although State Grid Xinjiang Company has leased 6MHz bandwidth in the Ku-band on the ChinaSat 6D satellite, existing satellite terminals suffer from high power consumption, high cost, protocol incompatibility, and major security risks, making it difficult to meet the demands of the electric power internet of things (IoT)[7–9]. Therefore, there is an urgent need to develop satellite IoT terminals, overcoming key technologies such as low demodulation threshold modulation, miniaturized integrated design, and strong electromagnetic anti-interference. Uniform specifications must also be established to solve the problem of real-time data transmission for electric power in areas without public network coverage, supporting the intelligent operation, maintenance, security, and stable operation of the Xinjiang power grid.

Electric Power Satellite IoT Private Network System Architecture and Terminal Design

A. Satellite-Terrestrial Collaborative Network Topology

Satellite-terrestrial integration is a core direction for 6G to overcome ground coverage limitations and achieve global ubiquitous connectivity. Through unified architecture and protocols, the satellite-terrestrial collaborative network deeply combines the wide coverage of space-based systems with the high capacity of ground-based systems, forming an all-round space-air-ground-sea integrated connectivity system[10–13]. Fig. 1 shows the networking diagram of the Electric Power Satellite IoT Private Network System.

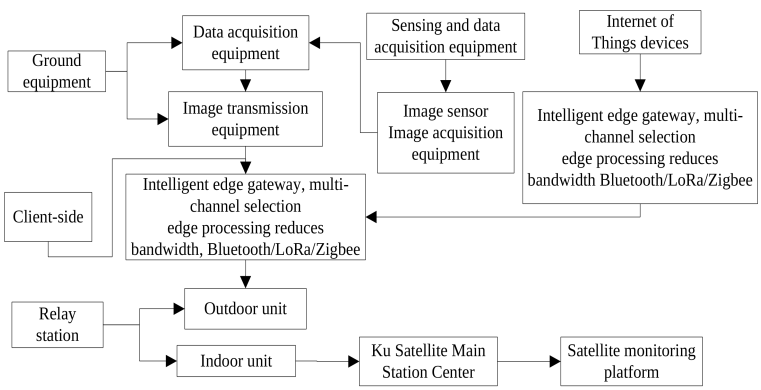

Figure 1. Networking Diagram of the Electric Power Satellite IoT Private Network System

The satellite-terrestrial collaborative network consists of three layers: space segment, ground segment, and user segment. The space segment comprises GEO, MEO, and LEO satellites, providing wide-area coverage and relay. The ground segment includes gateway stations, core network, and cloud resource pools, acting as a bridge between the space-based system and service platforms. The user segment contains satellite IoT terminals, sensors, and other devices. Xinjiang Electric Power adopts a "GEO for coverage, LEO for capacity" collaborative network, enabling millisecond-level intelligent switching and increasing bandwidth by 5 times compared to using only GEO[14–16].

The integrated electric power satellite IoT terminal is the core access device, operating in the Ku-band. It can establish data channels in areas without public networks, connecting collection devices and satellite master stations to transmit tower status data back to the electric power IoT platform. This terminal feature high integration, small size, low power consumption, strong environmental adaptability, supports multiple types of data backhaul, and provides reliable support for remote-area power online monitoring and emergency communication.

In practical validation at Xinjiang new energy stations, state grid Xinjiang electric power constructed a "Satellite + Terrestrial Mesh Network" collaborative architecture, integrating the wide coverage advantage of satellites with the local flexible networking capability of terrestrial mesh networks, achieving extended satellite signal coverage.

B. Integrated Terminal Hardware Design

The integrated electric power satellite IoT terminal is the core hardware achievement of this paper, characterized by high integration, low power consumption, and strong environmental adaptability. The terminal uses a Ku-band flat-panel high-gain microstrip antenna with a profile thickness of only 100mm. The overall dimensions are 317mm $\times$ 243mm $\times$ 100mm, weight $\leq$ 4.5kg, achieving significant miniaturization compared to traditional antennas. The RF front-end uses a Gallium Nitride (GaN) power amplifier with output power $\geq$4W and efficiency $>$50% in the Ku-band, paired with a low-noise amplifier to form a complete transceiver chain. The modem is based on a software-defined radio architecture, supporting TDMA/TDM schemes, with forward/return rates up to 1000kbps/500kbps, and includes automatic power control functionality.

Each module is integrated into a lightweight metal enclosure using 3D heterogeneous integration. The total operating power consumption is $\leq$30W, standby power consumption $<$5W. It features only a single aviation composite interface, allowing for both sleep and remote wake-up. The terminal achieves an IP66 protection rating and can operate stably in extreme temperatures ranging from -40°C to +60°C, as well as in strong sandstorms and high-humidity environments, meeting the requirements for unattended deployment on transmission towers. Fig. 2 shows the integrated electric power satellite IoT Terminal.

C. Communication Protocol and Data Flow

The integrated electric power satellite IoT terminal adopts TDM/TDMA multiple access. The forward link (master station $\rightarrow$ terminal) uses TDM broadcast, BPSK modulation, 1/5 rate QC-LDPC coding, with a demodulation threshold ≤ -15dB. The return link (terminal $\rightarrow$ master station) uses TDMA bursts, QPSK modulation, 1/3 Turbo coding, combined with 12x direct sequence spreading, supporting up to 4 sub-carriers for CDMA multiplexing, with a demodulation threshold ≤ -17dB. The modem supports

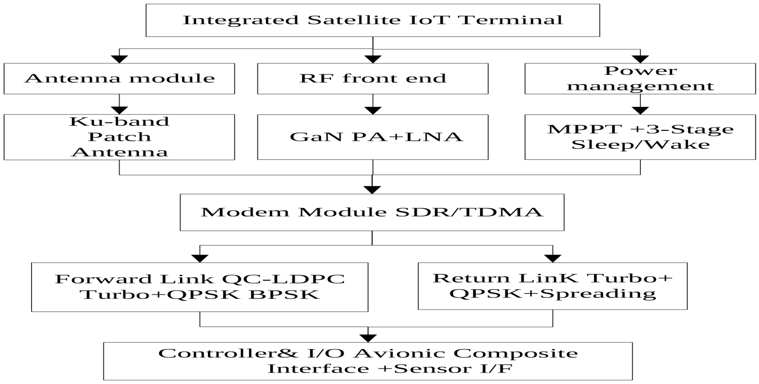

Figure 2. Integrated Electric Power Satellite IoT Terminal

forward rates up to 1000kbps and return rates up to 500kbps, with a roll-off factor of 0.05, and includes automatic power control. The parameters of the terminals listed in the Table 1.

The front-end acquisition device sends monitoring data to the terminal. After compression and SM4 encryption, the data is modulated to the Ku-band within a TDMA time slot, amplified by the GaN PA, and transmitted via the antenna to the satellite. The satellite frequency-converts the signal and broadcasts it to the ground master station. After demodulation and decryption, the data is forwarded through the core network to the electric power IoT platform, completing the end-to-end link closure.

Table 1. Terminal Uplink/Downlink Communication Protocol Parameters

Link Direction	Access Method	Coding Scheme	Modulation	Spreading	Demodulation Threshold
Forward (Gateway Terminal)	TDMBroadcast	1/5QCLDPC	BPSK	None	≤ -15 dB
Return (Terminal $\rightarrow$ Gateway)	TDMA Burst	1/3Turbo	QPSK	12×Spreading	≤ -17 dB

Key Technologies for Low Power Consumption and High-Reliability Communication in Terminals

A. Hardware Energy Saving Optimization Strategy

Targeting the solar-battery hybrid power supply scenario for field power equipment, terminal hardware energy-saving design focuses on three aspects: the component selection, the power management and the thermal/EMC design. Gallium Nitride (GaN) power amplifier devices are selected, achieving Power Added Efficiency (PAE) meeting: PAE $\geq$ 50% at Pout = 4W in Ku-band. Baseband processing uses a low-power FPGA supporting Dynamic Voltage and Frequency Scaling (DVFS). The power consumption model is:

$$P_{total} = P_{dynamic} + P_{leakage} \tag{1}$$

$$P_{dynamic} \propto C \times V^2 \times f \tag{2}$$

In terms of power management, a high-speed PA dynamic on/off switch is designed based on the TDMA return scheme. The power consumption reduction ratio is:

$$\eta = \frac{P_{const} - P_{dynamic}}{P_{const}} \times 100 \tag{3}$$

An integrated MPPT controller uses:

$$P_{PV} = U_{PV} \times I_{PV} \tag{4}$$

To achieve seamless day/night switching between solar power and stored battery energy. For thermal and EMC considerations, a lightweight metal enclosure is used. Thermal grease is filled between key heat-generating components and the enclosure, with thermal resistance meeting $E_{th} = \frac{\Delta T}{P_{loss}}$, ensuring stable operation in environments from -40°C to +60°C. The terminal achieves an IP66 protection rating, overall achieving low energy consumption and long endurance.

B. Adaptive Sleep Scheduling Algorithm

To achieve the standby power consumption target of no more than 5W, the terminal is designed with a three-level sleep/wake-up mechanism:

The scheduling strategy is as follows. At first, based on the periodicity of power monitoring services, the terminal sets an RTC timer. Secondly, it wakes up 500ms before the scheduled time, completes data acquisition, compression, and encryption, transmits within the allocated TDMA time slot, and then immediately returns to deep sleep. At last, when triggered by an event, the terminal can be woken up remotely and actively request additional time slots.

C. Anti-Interference Coding and Modulation Technology

In the complex electromagnetic environment of power satellite communication, this paper proposes the following anti-interference scheme:

The forward link uses rate 1/5 QC-LDPC coding and BPSK modulation, with a demodulation threshold $r \leq -15dB$. The return link uses rate 1/3 Turbo coding, QPSK modulation, and 12x direct sequence spreading. The spreading processing gain is:

$$G_p = 10 \log_{10}(SF) \approx 10.8dB \tag{5}$$

Supporting up to 4 sub-carriers for CDMA, the equivalent SNR improvement is:

$$SNR_{eq} = SNR_{in} + G_p + G_c \tag{6}$$

Where input SNR: $SNR_{in} = -2dB$, coding gain $G_c \approx 5dB$, resulting in $SNR_{eq} \approx +8.8dB$. Simultaneously, the terminal adaptively selects BPSK/QPSK/8PSK modulation and code rate $r \in [1/5,\ 1/2]$ based on real-time carrier-to-noise ratio (CNR), with a demodulation threshold step $r \leq -0.5dB$. The spectral efficiency is:

$$\eta = \max_{mod,r} r \log_2(M) \tag{7}$$

Thus, maximizing spectral efficiency while ensuring anti-interference capability.

cosine-Gaussian beam

A. Theoretical Gain Analysis of Low Demodulation Threshold Algorithm

According to the Shannon channel capacity formula:

$$C = B \log_2(1 + SNR) \tag{8}$$

The required signal-to-noise ratio is $SNR = -12\ dB$, i.e., the linear value $SNR = 10\hat{} - 12/10 = 0.0631$

Substituting gives: C ≈ 17.5 kbps

This theoretical limit is higher than the minimum required rate of 10 kbps for power monitoring, indicating that reliable communication is theoretically achievable at −12 dB. The comparison results of the different coding schemes are showed in the Fig. 3.

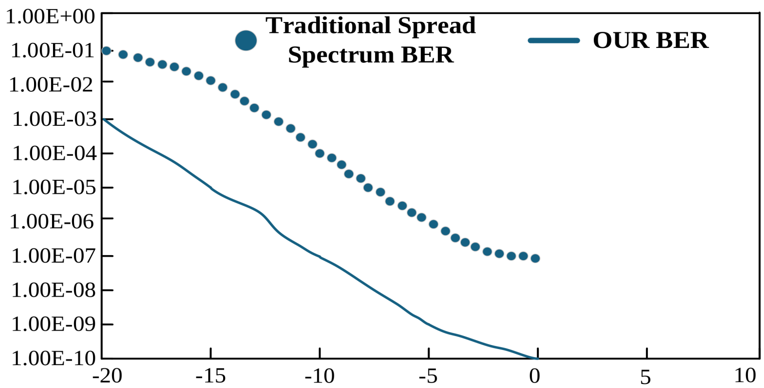

Figure 3. Theoretical BER-SNR Performance Comparison Curves for Different Coding Schemes

After adopting the combined QC-LDPC and spreading scheme, the practically achievable coding gain is about 5-6 dB, meaning the required SNR can be further reduced to about −17 dB, far superior to traditional spreading schemes (which require −10 dB for the same bit error rate without LDPC). Therefore, the scheme in this paper meets the design goal of a demodulation threshold not exceeding −12 dB.

B. Power Management Strategy and Communication Delay Performance Simulation

Using the three-level sleep scheduling, set a typical service model: transmit once per hour, work for 10 seconds each time, and remain in deep sleep for the remaining 3590 seconds.

The average power consumption calculation formula is:

$$P_{avg} = \frac{P_{work} \cdot T_{work} + P_{sleep} \cdot T_{sleep}}{T_{cycle}} \tag{9}$$

Substituting the values: $P_{work} = 30W$, $T_{work} = 10s$, deep sleep power $P_{sleep} = 1W$, sleep time $T_{sleep} = 3590s$; cycle $T_{cycle} = 3600s$. The average daily power consumption of the proposed scheme is 25.9 Wh, achieving approximately 94.6% energy saving compared to traditional VSAT terminals. This can meet the requirement for the solar power system to operate for more than 7 days under continuous cloudy and rainy weather. The power consumption comparison is shown in Table 2:

Table 2. Power Consumption Comparison Table

Terminal Type	Operating Power	Stand By Power	Average Daily Power	Energy Saving Ratio
VSAT Terminal	≥80 W	≥20 W	480Wh	—
Proposed design	≤30 W	≤1 W	25.9 Wh	94.6%

To verify whether the link delay meets the real-time requirements of electric power services, a cross-regional power site satellite communication scenario was simulated using the Hypatia simulation platform, simulating data transmission between typical Xinjiang grid sites. The simulated end-to-end round-trip time (RTT) results are shown in the figure. The link RTT stabilizes between 90-115ms, far lower than the 500ms requirement, ensuring real-time backhaul of power monitoring data. So, the RTT simulation results are listed in the Fig.4.

C. Terminal Congestion Control and System Reliability Simulation Verification

To address issues of time-varying satellite links and multiple terminals competing for access, which can easily lead to congestion and packet loss, the terminal TCP congestion control and the overall network delay characteristics are simulated and verified in this paper. Then the congestion test results are showed in the Fig. 5.

As shown in Fig. 5, under time-varying satellite link and path switching conditions, the TCP congestion window can quickly converge following the link capacity. Packet reordering causes only brief fluctuations, demonstrating good transmission stability.

As shown in Fig. 6, when multiple terminals access concurrently, the global delay stabilizes between 0.5-3 seconds, with no obvious congestion or blocking. Combined with the anti-interference and low demodulation threshold design, the system can meet the high-reliability transmission requirements of the Electric Power IoT.

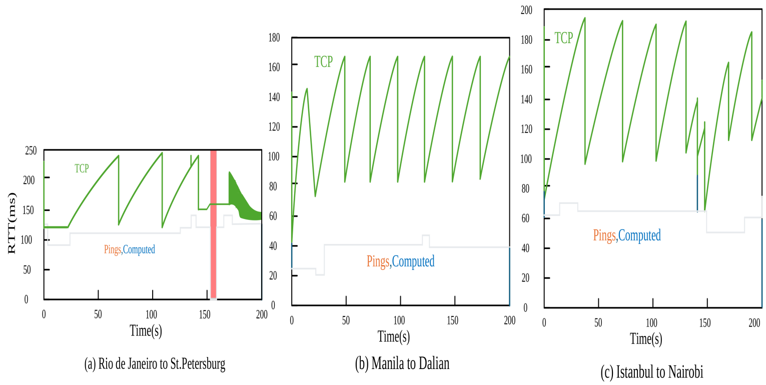

Figure 4. RTT Simulation Results

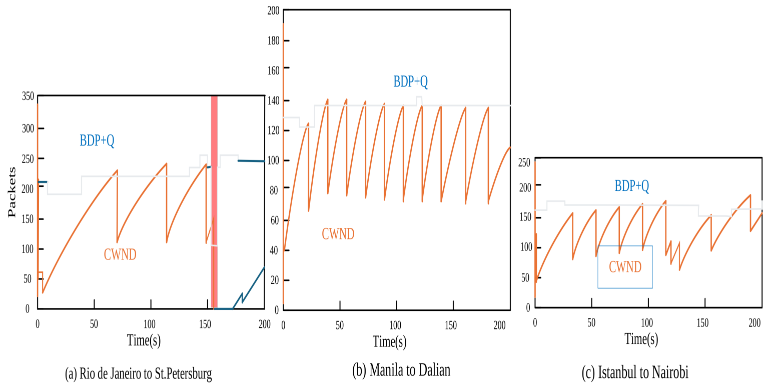

Figure 5. TCP Congestion Window Test Results

Upon power-on, the terminal sequentially completes initialization, satellite synchronization, and network registration. When there is no task, it enters deep sleep to achieve ultra-low power consumption. It wakes up quickly upon periodic data collection or alarm event triggers, completes data transmission, and automatically enters a fault self-healing state if continuous transmission fails, overall achieving a closed-loop operation of low power consumption and high reliability.

Conclusion

Aiming at the communication requirements for transmission line monitoring in areas without public network coverage, relying on Ku-band satellite resources, and focusing on the two key technical challenges of energy efficiency optimization and low demodulation threshold, this paper has completed the following work. At first, using the GaN power amplifier, TDMA time slot PA switching and the three-level sleep scheduling, we optimized the hardware energy saving. So, the terminal's operating power consumption is no more than 30W, standby power consumption no more than 1W, achieving over 90%

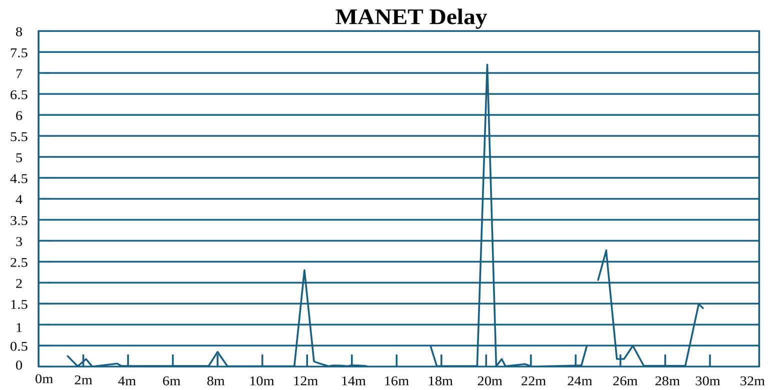

Figure 6. Global Delay

energy saving compared to traditional VSAT terminals. Then, introducing the very low-rate QC-LDPC codes and a combination of 12x spreading and CDMA, the theoretical demodulation threshold is as low as -17dB, meeting the -12dB target, effectively coping with strong electromagnetic interference on transmission lines. At last, we provided a complete terminal working state transition diagram and data flow, ensuring seamless integration with the electric power IoT platform. The satellite terminal designed in this paper can effectively solve the payload problem in power grid communication scenarios and can provide reliable technical support for subsequent research.

Author Contributions

The corresponding author is Gang Liang

References

[1] L. Liu, W. Li and F. Zhou, "Enhancing 6G IoT Communications: UAV Relayed Satellite D2D with Large Language Model Optimization," in IEEE Communications Magazine, vol. 63, no. 11, pp. 90-96, November 2025, doi: 10.1109/MCOM.001.2500196.

[2] V. Fidele Adanvo, S. Mafra, S. Montejo-Sánchez, F. Augusto Tondo and R. Demo Souza, "Analytical Modeling of Slotted Aloha-Based Direct-to-Satellite-IoT Sensor Networks Over Nakagami-m Fading Channels," in IEEE Sensors Journal, vol. 26, no. 2, pp. 3264-3277, 15 Jan.15, 2026, doi: 10.1109/JSEN.2025.3635197.

[3] Q. Wang et al., "Energy-Efficient Task Split and Resource Allocation in LEO-Satellite-Assisted IoT Network," in IEEE Internet of Things Journal, vol. 11, no. 21, pp. 34519-34527, 1 Nov.1, 2024, doi: 10.1109/JIOT.2024.3441718.

[4] A. Talgat, M. A. Kishk and M. -S. Alouini, "Maximizing Uplink Data Transmission of LEO-Satellite-Based Wireless-Powered IoT," in IEEE Internet of Things Journal, vol. 11, no. 17, pp. 28975-28987, 1 Sept.1, 2024, doi: 10.1109/JIOT.2024.3405661.

[5] A. K. Dwivedi, S. Chaudhari, N. Varshney and P. K. Varshney, “Performance Analysis of LEO Satellite-Based IoT Networks in the Presence of Interference,” in IEEE Internet of Things Journal, vol. 11, no. 5, pp. 8783-8799, 1 March1, 2024, doi: 10.1109/JIOT.2023.3321574.

[6] H. Zhang, X. Han, C. Xing, H. Chen and J. Zhao, “Analysis of Uplink Transmission Scheduling Strategies for LoRa-Based Direct-to-Satellite IoT Networks Using Deep Reinforcement Learning,” in IEEE Transactions on Green Communications and Networking, vol. 10, pp. 1279-1292, 2026, doi: 10.1109/TGCN.2025.3622318.

[7] N. Biswas, N. Saket Racherla, S. Chakraborty and A. Mukhopadhyay, “End-to-End Throughput Optimization in Integrated Satellite-IoT and Terrestrial Networks,” in IEEE Wireless Communications Letters, vol. 14, no. 10, pp. 3129-3133, Oct. 2025, doi: 10.1109/LWC.2025.3587146.

[8] Tian, L., He, C., Peng, M., & Li, X. (2024). Hydrogen evolution reaction in the hBNC/Janus MoSSe heterojunction: First-principles calculations. International Journal of Hydrogen Energy, 2024, 60, 369-377.

[9] P. Qin, D. Xu, L. Liu, M. Dong, S. Mumtaz and M. Guizani, “Joint Data Allocation and LSTM-Based Server Selection With Parallelized Federated Learning in LEO Satellite IoT Networks,” in IEEE Transactions on Network Science and Engineering, vol. 11, no. 6, pp. 6259-6271, Nov.-Dec. 2024, doi: 10.1109/TNSE.2024.3481630.

[10] Z. Yin et al., “UAV-Assisted Secure Uplink Communications in Satellite-Supported IoT: Secrecy Fairness Approach,” in IEEE Internet of Things Journal, vol. 11, no. 4, pp. 6904-6915, 15 Feb.15, 2024, doi: 10.1109/JIOT.2023.3313197.

[11] A. Talgat, M. A. Kishk and M. -S. Alouini, “Stochastic Geometry-Based Uplink Performance Analysis of IoT Over LEO Satellite Communication,” in IEEE Transactions on Aerospace and Electronic Systems, vol. 60, no. 4, pp. 4198-4213, Aug. 2024, doi: 10.1109/TAES.2024.3374718.

[12] Tian L, Hu J, He C, et al. hBNC/Janus MoSTe heterojunctions in photocatalytic water splitting for hydrogen production: A first-principles study[J]. Chemical Physics Letters, 2024, 856: 141587.

[13] Y. Shi, Q. Luo, S. Zhang, J. Wang and J. Liu, “Jamming Scheduling and Resource Allocation for Secure Communication in Massive LEO Satellite-Empowered IoT Network,” in IEEE Internet of Things Journal, vol. 13, no. 5, pp. 9849-9860, 1 March1, 2026, doi: 10.1109/JIOT.2025.3646153.

[14] Raydel Ortigueira, Samuel Montejo-Sánchez, Santiago Henn, Juan Fraire, Sandra Céspedes. Satellite Visibility Prediction for Constrained Devices in Direct-to-Satellite IoT Systems. IEEE Sensors Journal, 2024, 24 (16), pp.26630-26644.

[15] F. Zheng et al., “A Dual-Layer Deep Reinforcement Learning Routing Approach for Integrated UAV and Satellite IoT Networks,” in IEEE Internet of Things Journal, vol. 13, no. 3, pp. 3630-3644, 1 Feb.1, 2026, doi: 10.1109/JIOT.2025.3602147.

[16] K. RATHI, V. SHARMA, S. GUPTA, A. BAGWARI and G. S. TOMAR, “Home Appliances using loT and Machine Learning: The Smart Home,” *2022 14th International Conference on Computational Intelligence and Communication Networks (CICN)*, Al-Khobar, Saudi Arabia, 2022, pp. 329-332, doi: 10.1109/CICN56167.2022.10008294.

[17] A. K. Dwivedi, S. Chaudhari, N. Varshney and P. K. Varshney, “Performance Analysis of LEO Satellite-Based IoT Networks in the Presence of Interference,” in IEEE Internet of Things Journal, vol. 11, no. 5, pp. 8783-8799, 1 March1, 2024, doi: 10.1109/JIOT.2023.3321574.